Biomed Microdevices (2007) 9:681–694
DOI 10.1007/s10544-007-9077-z

Microfluidic self-assembly of live *Drosophila* embryos for versatile high-throughput analysis of embryonic morphogenesis

Gabriel T. Dagani · Kate Monzo · Jean R. Fakhoury · Chung-Chu Chen · John C. Sisson · Xiaojing Zhang

Published online: 17 May 2007

Abstract A method for assembling *Drosophila* embryos in a microfluidic device was developed for studies of thermal perturbation of early embryonic development. Environmental perturbation is a complimentary method to injection of membrane-impermeable macromolecules for assaying genetic function and investigating robustness in complex biochemical networks. The development of a high throughput method for perturbing embryos would facilitate the isolation and mapping of signaling pathways. We immobilize *Drosophila* embryos inside a microfluidic device on minimal potential-energy wells created through surface modification, and thermally perturb these embryos using binary laminar flows of warm and cold solutions. We self-assemble embryos onto oil adhesive pads with an alcohol surfactant carrier fluid (detachment: 0.1 mL/min), and when the surfactant is removed, the embryo-oil adhesion increases to ~25 mL/min flow rates, which allows for high velocities required for sharp gradients of thermal binary flows. The microfluidic thermal profile was numerically characterized by simulation and experimentally characterized by fluorescence thermometry. The effects of thermal perturbation were observed to induce abnormal morphogenetic movements in live embryos by using time-lapse differential interference contrast (DIC) microscopy.

Keywords Microfluidic · Self-assembly · (Polydimethylsiloxane) PDMS · *Drosophila* embryo · Thermal perturbation · Embryogenesis · Cellularization

G. T. Dagani · J. R. Fakhoury · X. Zhang (✉)
Department of Biomedical Engineering,
The University of Texas at Austin, 1 University Station,
ENS 12, Austin, TX 78712-0238, USA
e-mail: John.Zhang@engr.utexas.edu

G. T. Dagani · J. R. Fakhoury · X. Zhang
Microelectronics Research Center,
The University of Texas at Austin, Austin, TX, USA

K. Monzo · J. C. Sisson
Section of Molecular Cell & Developmental Biology,
The University of Texas at Austin, Austin, TX, USA

C.-C. Chen
Medical Electronics and Device Technology Center, Industrial Technology Research Institute, Taiwan, Republic of China

1 Introduction

High-throughput methodologies are practical screening techniques for isolating and mapping genetic signaling pathways in living organisms. Practices common for mapping signaling pathways include injecting small molecule inhibitors (Carthew 2001), observing the morphology of genetic mutants, and perturbing the environment around an organism with extreme artificial conditions. Model organisms, such as *Drosophila melanogaster*, are typically used for these experimental investigations due to its relatively short reproductive cycle, its relatively small genome, and its amenability to sophisticated biochemical, genetic, and cell biological analysis (Rubin and Lewis 2000). The first comprehensive characterization of genes that regulate cellular function and differentiation in a complex organism was performed in early *Drosophila* embryos (Nusslein-Volhard and Wieschaus 1980). This discovery has since led to the mapping of many other regulatory responses in *Drosophila* embryos using engineered perturbation (Niemuth and Wolf 1995; Eldar et al. 2004; Yucel and Small 2006).

Technology used for observing cell morphology is crucial for accurately mapping genetic networks. "Labs-on-a-chip," such as microfluidic devices, are emerging

platforms capable of expanding conventional cell culture using biomimetic surfaces and accurate chemical delivery at high spatial-temporal resolution. Laminar flows in microchannels can generate chemical (Kamholz et al. 1999), mechanical (Brown 2000; Walker et al. 2004), optical (Debarre et al. 2004), and thermal gradients to induce regulatory behavior in *Drosophila* embryos. Further investigations into chemical pathways will require the orchestration of these variables to expose the critical elements that manage robustness in genetic networks. Recently, microfluidic devices were used to perturb a *Drosophila* embryo manually positioned between two distinct flows of warm and cold buffer (Lucchetta et al. 2005). The simultaneous contrasting conditions tested the effects on embryo development. By switching between temperatures, it was observed that embryos fully hatched and developed into normal offspring. It was also found that the alignment of the embryos in the channel is crucial for the perturbation at the microscale with high precision (Lucchetta et al. 2006). However, the current manual embryo placement technique can potentially cause large embryo misalignment, and the procedure is time consuming. In addition, performing experiments on arrays of embryos simultaneously is desirable for high throughput screening. We developed a self-assembly technique for immobilizing embryos on an open substrate (Zhang et al. 2005), through patterning sequentially viscous fluorocarbon oil and thiol monolayers (SAMs) on gold pads. The embryos adhered to the oil, and were immobilized by capillary force. In this paper, we extend the self-assembly method into the microfluidic domain for thermal perturbation experimentation.

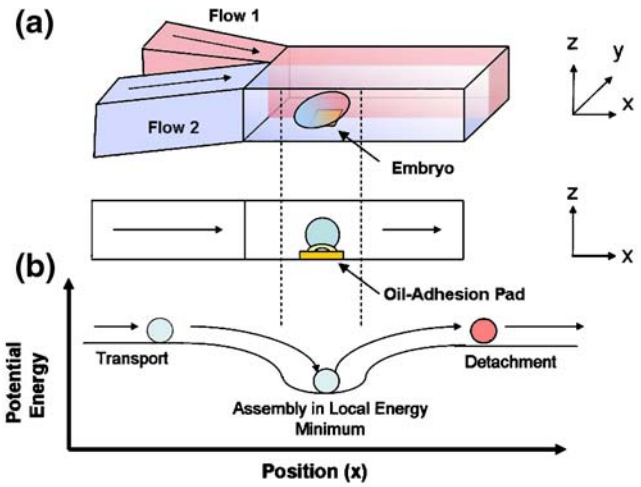

Fig. 1 Self assembly of embryos on "energy wells" within the microchannel. (**a**) Embryo assembled to pad with binary (for example, hot and cold) flows surrounding it. (**b**) Principle of self assembly of embryo in "energy well." Oil-adhesion pads are modeled as energy wells for immobilizing an embryo in the microchannel. Embryo is pulled into pad via capillary force from the oil adhesive. Embryo is immobilized until sufficient force overcomes the adhesion and detachment occurs

The proposed microfluidic assembly depends on fluidic shear force and the adhesive strength of the assembly bridge. Three steps of embryo self-assembly include embryo transport, embryo assembly, and embryo detachment (Fig. 1). The assembly process follows the minimal potential-energy principle: a particle (embryo) makes initial contact with adhesive pad and incurs initial potential energy. Once the particle is in contact, it seeks a minimal energy state to achieve thermodynamic stability. A detachment force, such as the fluidic shear force larger than the adhesion force, is required to move the particle away from the influence of the energy well (Kendall 1971). We model the interfacial tension stresses between the embryo, the oil bridge, the surrounding media, and the assembly pad, and investigate the effect of surfactants and carrying fluid of different densities on the assembly. The microfluidic thermal profile is numerically characterized by simulation and experimentally characterized by fluorescence thermometry. Finally, we demonstrate how this microfluidic device can be used to study cellularization, a complex morphogenetic event that occurs during early *Drosophila* embryogenesis. Effects of thermal perturbation on cellularization were observed using time-lapse microscopy.

2 Principles of operation

2.1 Diffusion, gradients and mixing

We use microfluidics to expose an embryo to an environment that emulates natural growth conditions and introduces extreme artificial conditions for perturbation. Manipulating and culturing embryos is very different from culturing cells, where the most simple noticeable difference is the size. A yeast cell is around 1 μm in diameter, and a typical blood cell is 10 μm in diameter. Embryos can range from a 100 μm mouse embryo to a 400 μm *Drosophila* embryo and even up to a 4 mm human embryo (at 13 weeks). While small cells may remain unaware of its microfluidic environment, an embryo is similarly scaled and closely affected by channel geometry (Sugihara-Seki 2000, 2001).

Microfluidic gradients are described by the Peclet number, which is a ratio of convective mixing versus diffusive mixing. Convection is represented by the product of velocity and characteristic length, while diffusion is represented by the diffusion coefficient of the miscible fluids. Typical flow rates of 10 cm/s within a microchannel have a large Peclet number (~10^4), which indicates that convection is dominant and diffusion is limited. For example, two aqueous fluids have a diffusion coefficient

between 10^{-5}–10^{-7} cm^2/s, and flow together at a rate of 1 cm/s inside a 100 μm wide microchannel. With a diffusion coefficient of 10^{-6}, these flows are described by a Reynolds number of ~1 (Eq. 1), and a Peclet number of $\sim 10^4$ (Eq. 2). Based on these properties, 100 s (Eq. 3) or a ~100 cm (Eq. 4) mixing length is required to completely diffuse two aqueous solutions into a 50–50 mixture.

$$Re = \left(\frac{\rho V d}{\mu}\right) = \left(\frac{\left(10^3 \frac{kg}{m^3}\right)\left(1\frac{cm}{s}\right)(10^{-2}cm)}{0.001\,Pa \cdot s}\right) = 1 \quad (1)$$

$$Pe = \left(\frac{Vd}{D}\right) = \left(\frac{\left(1\frac{cm}{s}\right)(10^{-2}cm)}{10^{-6}\frac{cm^2}{s}}\right) = 10^4 \quad (2)$$

$$\delta \sim \sqrt{Dt_D} \Rightarrow t_D \sim \frac{\delta^2}{D} \sim \frac{(10^{-2}cm)^2}{10^{-6}\frac{cm^2}{s}} \sim 100s \quad (3)$$

$$L_{mix} = (V \cdot t_D) \sim \left(1\frac{cm}{s}\right)(100s) \sim 100cm \quad (4)$$

ρ fluid density
V velocity
D diffusion coefficient
t_D diffusion time
μ dynamic viscosity
d dynamic viscosity
δ diffusion length
L_{mix} mixing length

The mixing length can be reduced by decreasing the flow rate or by increasing the temperature of the fluids (Ismagilov et al. 2000). Decreasing the flow-rate inside a microfluidic channel increases the amount of time for species interaction, and decreases the length (but not the time) required for full diffusion (Hatch et al. 2001). Also, the temperature increase reduces the effective viscosity and increases the diffusion coefficient, which decreases the mixing length.

Our perturbation experiments require a discrete temperature profile with narrow mixing regions across the entire embryo in order to observe the effects of subjecting one half of the embryo to one condition and the other half to a different condition. To sharpen a thermal gradient, the convection should be increased, and the thermal diffusivity decreased. Thermal diffusivity can also be reduced by using a different fluid such as oil, which has a larger heat capacity (Eq. 5). Water has a thermal conductivity of 0.60 W/(m·K), glycerol's thermal conductivity is 0.29 W/(m·K), and mineral oil is only a quarter that of water 0.14 W/(m·K). However, it should be noted that both glycerol and mineral have reduced oxygen permeability, and much greater viscosity.

$$\alpha = \frac{\kappa}{\rho \cdot c_p} \quad (5)$$

α thermal diffusivity
c_p heat capacity
κ thermal conductivity
ρ fluid density

2.2 Microfluidic self-assembly

Self-assembly is the joining of two or more entities in an arrangement designated by thermodynamic stability, and generally requires a part to be assembled on a compatible energy well. Capillary force, magnetic force (Grzybowski et al. 2001; Oliver et al. 2001), hydrophobicity (Srinivasan et al. 2001), and electrostatic force (Caruso et al. 1998) are all potential actuation methods for assembly. During the process of self-assembly, pieces are introduced into a closed system (Fang and Böhringer 2006) and the system is bombarded with energy such as vibration (Bernstein et al. 2002), heat (Xiong et al. 2003), or chemical reaction (Freire and Coelho-Sampaio 2000). These disturbed pieces move in a Brownian fashion until they converge into energy wells where they are most thermodynamically stable.

Fluidic self-assembly (FSA) is a subset of self-assembly that uses liquids to transport micro-scale objects for delivery to energy wells. Typically, the fluids also reduce corresponding gravitational effects, which allow competing surface and electrostatic forces to govern the means of assembly. Smith et al. (Yeh and Smith 1994; Talghader et al. 1995) demonstrated this principle in 1994 for microelectronic assembly of circuit-blocks using literal wells to perform shape-directed placement. The principles behind fluidic self-assembly can be divided into two categories: transportation and immobilization. Transportation of spherical and ellipsoidal particles is described by stokes flow and buoyancy models. Immobilization of particles is described using an "energy well" model of adhesive pads. The assembly force depends on the particle penetrating the adhesive-liquid boundary. Once a particle is immobilized, mechanical forces applied must be greater than the adhesive force for detachment of the particle to occur.

The surface wetting equation (Eq. 6) describes the net interfacial energy between a surface and a spreading liquid in a non-miscible fluid environment. Surface wetting between two substrates is known as capillary force, and is capable of pulling two small objects closer together as a

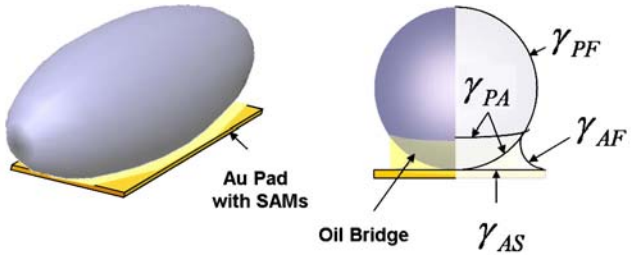

Fig. 2 Diagram of embryo assembled to pad with various interfacial tensions. γ_{ij}: Interfacial tension where i and j indicate the two touching fluid surfaces, P Particle, A Adhesive, S SAMs, F Fluid

combined result of van der Waals dispersive forces and hydrogen bonding (Peppas and Sahlin 1996). The same surface wetting equation can also be extended to describe the capillary force between two different surfaces in contact with an adhesive bridge (Eq. 7) (Zhang et al. 2005). For these equations, the variables represent the particle surface (P), the liquid adhesive (A), the surrounding carrier fluid (F), and the substrate surface (S) (see Fig. 2).

$$E = A_{AF}\gamma_{AF} + A_{PF}\gamma_{PF} + A_{PA}\gamma_{PA} \tag{6}$$

$$E = A_{PF}\gamma_{PF} + A_{PA}\gamma_{PA} + A_{AF}\gamma_{AF} + A_{SF}\gamma_{SF} + A_{SA}\gamma_{SA} \tag{7}$$

E total surface energy between fluid surfaces
A_{ij} interfacial area between surfaces i and j
γ_{ij} interfacial tension between surfaces i and j

Assuming the particle is capable of making intimate contact with the adhesive energy well, the interfacial energy between the adhesive and the particle should be smaller than the energy between the particle and the carrier fluid. A low interfacial energy between the particle's surface and the adhesive promotes the surface wetting of the particle, and has the potential for pulling the particle into the energy well for assembly. As the particle assembles, the area between the different surfaces changes so that the substrate and particle surfaces increasingly overlap (Eq. 8).

$$\Delta E = \Delta A_{PF}(\gamma_{PF} - \gamma_{PA}) + \Delta A_{AF}\gamma_{AF} + \Delta A_{SF}(\gamma_{SF} - \gamma_{SA}) \tag{8}$$

ΔE change in surface energy

Because hydrophobic surfaces exposed to the fluidic environment are a source of instability, orientation of self assembled particles can be predicted. Böhringer et al. (Xiong et al. 2003) explained this orienting ability (Eq. 9) by demonstrating that a minimal energy state is directly proportional to the overlap between the binding site and the self-assembled-particle.

$$\Delta E \propto A_S\gamma_S + A_P\gamma_P - 2(A_S\gamma_S \cap A_P\gamma_P) \tag{9}$$

A area of intersecting immiscible fluids

Adhesion is described as the force required to separate two surfaces. The work involved to separate these surfaces is equal to twice the net interfacial energy (Eq. 10). Because it is impossible to perfectly detach two surfaces with no wasted energy, over-estimating the detachment force is widely accepted whereas all unaccounted energy is considered dissipated by viscous forces as the surfaces move apart (Kendall 1971).

$$W_{\text{detach}} \geq 2\gamma_{PS} \cdot A \tag{10}$$

W_{detach} the work required to separate two surfaces

A particle can be removed from its energy well by incurring a mechanical force exceeding the adhesive-viscous force outside the well's influence. Self-assembly of embryos in microchannels is similar to fluidic assembly except it also includes the option for manipulating the embryo after assembly. Using surfactants or liquids of different densities have a dramatic impact on the required force for assembly and detachment.

3 Device design and fabrication

3.1 Device design

Our perturbation experiments require a discrete temperature profile with narrow mixing regions across an entire embryo. The goals of the device design include (a) reliable embryo deposition, (b) good adhesion of embryo to pad during extended pressured flow, (c) well-controlled orientation of self-assembled embryos, (d) sharp perturbation gradients, and (e) unobstructed viewing of embryo growth in the microchannel using microscopy. The Y-channel is the most simple and intuitive device geometry for introducing binary flows. Height and width constraints of the device's main channel are on the same order as the size of a *Drosophila melanogaster* embryo. Females oviposit fertilized eggs, which are prolate spheroid shaped with an average width of 250 μm and a length of 400 μm.

Oil-adhesion pads are modeled as energy wells for immobilizing an embryo in the microchannel. The influence of pad geometries on the embryo orientation correlates with the maximum surface area overlap. The initial work on self-assembly pads was based on the work by Zhang et al.

For this research, the immobilization technique is transferred into a microfluidic environment instead of on an open substrate. Pad geometries are designed with one longer axis of surface area to influence embryo orientation.

3.2 Device fabrication

Two sets of microfluidic devices were fabricated, a silicon based device, and a glass based device (Fig. 3). Silicon based devices were used for self-assembly experiments because its opaque backdrop allowed excellent contrast for embryo visualization from a top-view stereomicroscope. Glass cover-slip bases were used for the experiments requiring inverted microscopy where the device was illuminated from the top and viewed from the bottom. Polydimethylsiloxane (PDMS) (Silgard 184, Essex Group, Inc.) was used as the primary channel material for both platforms because it is rapidly reproducible, and transparent. The method for fabricating the silicon device is identical to the method for fabricating the glass device, except the glass coverslips are replaced by single-side polished 3 in. silicon wafers.

The microchannel fabrication process is based on the rapid prototyping technique (Anderson et al. 2000). In this technique, SU8 photoresist (Microchem Corp.) is patterned photolithographically on a single side polished wafer (Fig. 3(a),(b)). Depending on the channel height specification for our device, SU8-2100 (~250 microns) or SU8-2150 (~500 microns) may be required. The photolithography process is provided by the Microchem Corporation in their product literature (Microchem-Corporation 2006). Polydimethylsiloxane (PDMS) is then shaped over the SU8 master mold, cured at 100°C for ~1 h, and peeled off the mold to form the microchannel.

Large glass coverslips (35×50 mm, Fisher Science) are cleaned using a standard piranha acid clean, followed by a quick 20 s (40:1) hydrofluoric (HF) acid dip. The glass slides are rinsed in water and blown dry with nitrogen and kept in a clean dry place. HDMS priming solution (Microprimer, Microchem Corp.) is applied at 3,000 RPM for 30 s. The photoresist AZ-5209E (Arizona Chemical Corp.) is then spun at 3,000 RPM for 30 s. The glass is baked at 90°C for 1 min, exposed to UV for 20–25 s at 10 mJ/cm^2, and baked again for 1 min. Patterns are developed in AZ-726MIF developer for 60 s, or until patterns are well defined (Fig. 3(c)). The glass is then rinsed in water and hard-baked at 65°C for more than 1 h.

Metal deposition is performed using a CHA E-beam evaporator. Approximately 20 Å of chromium is deposited as an adhesive layer to glass, and approximately 75 Å of gold is deposited on top of the chromium. After metal evaporation, slides are placed in an acetone bath for 5–15 min to remove photoresist and 'lift-off' the excess metal (Fig. 3(d)). The glass is ultrasonicated for a few seconds to

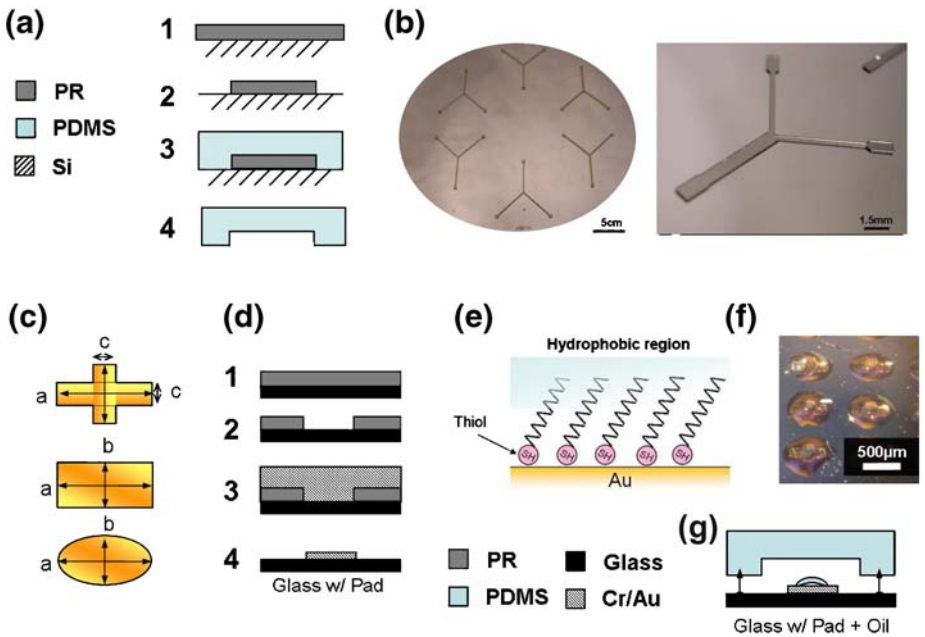

Fig. 3 Fabrication process. (**a**) Fabrication of the PDMS channel (1) Apply SU8 to silicon substrate. (2) Pattern the photoresist. (3) Pour and cure the PDMS over the mold (4) Peel off the SU8. (**b**) Photos of wafer with SU8 mold for channel. (**c**) Geometries of self assembled pads a=400 μm, b=200 μm, and c=50 μm. (**d**) Fabrication of the gold pads (1) Apply AZ-5209E onto glass. (2) Pattern photoresist. (3) Deposit chromium and gold. (4) Lift off photoresist with acetone. (**e**) Diagram of SAMs on gold (**f**) Micrograph of self assembly pads (*truncated cross*) covered in oil. (**g**) Plasma Bonding of PDMS channel to glass with oil covered thiol coated gold pads

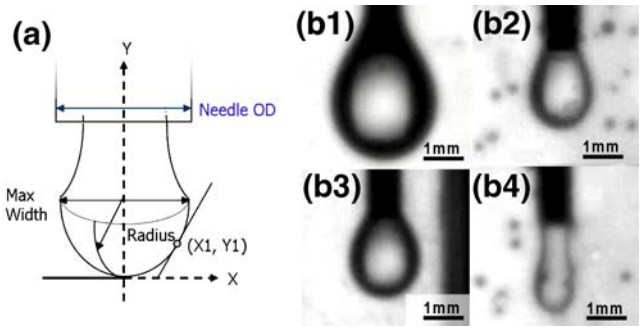

Fig. 4 Interfacial tension measured by pendant drops measurement in a cuvette of water. (**a**) Measurement criteria for performing pendant drop measurement. (**b**) Micrographs of oil pendant drops in a cuvette of fluid. (1) Oil in water; (2) Oil in 50% ethanol; (3) Oil in 50% methanol; (4) Oil in 95% ethanol

remove clinging particles. The slides are then cleaned in a piranha solution. A piranha clean makes glass hydrophilic for up to 72 h if hermetically sealed, or for 24 h if left exposed to air. After liftoff, a thiol application is carried out by submersing the substrate overnight in 15 mM octadecanethiol (ODT) dissolved in ethanol. This creates a self assembled monolayer (SAM) of thiol functionalized hydrocarbon strands coated over the gold surface. Self-assembled monolayers on the gold pad provide a detectable surface energy boundary between the pad and the substrate when doused in water.

Halocarbon 700 oil is made of poly-chlorotrifluoro-ethylene (CAS 9002-83-9) and is sold by the Halocarbon Products Corporation. Halocarbon oil (HCO) is commonly used as an inert medium during the manipulation of *Drosophila* embryos because it allows oxygen to permeate while keeping the dechorionated embryos from drying out (Halocarbon-Products-Corporation 2006). The purpose for patterning gold pads onto glass is to differentiate hydrophobic islands from a hydrophilic substrate. However, the ODT application is more effective on silicon than glass for differentiating a hydrophilic substrate (Fig. 3(e)). Glass requires a piranha cleaning to substantially differentiate the substrate from the patterned gold pads. Halocarbon oil can be applied to the substrate and pads and then isolated to the gold pads by a generous rinse of water (Fig. 3(f)).

Methods for combining the PDMS channel to the glass substrate with the self assembly pads are well characterized in literature (Anderson et al. 2000). An oxygen plasma is used to dry etch the surface of the glass and PDMS (Fig. 3(g)). Depending on the device used for performing the oxygen plasma (Plasma RIE, or March Asher), the plasma recipe may vary. After pushing the glass and PDMS together, the entire device is placed on a hot plate to complete the bonding process.

4 Experimental setup and results

4.1 Microfluidic assembly of embryos

The adhesion of the embryo to the oil pad is a direct result of the composite surface energies between the embryo, the pad, the buffer, and the oil. These surface energies are simulated using "Surface Evolver," a software developed by Ken Brakke (Brakke 2005). General parameters include the size of the embryo, the size of the pad, the amount of oil, and the relative interfacial energies and contact angles for the oil and embryo in water or alcohol.

4.1.1 SAMs modeling and simulation

To simulate the surface energies for alcohol and Halocarbon oil, we require the interfacial surface tensions between the embryo, oil, SAMs, and glass in alcohol. This can be done by using pendant drop analysis as shown in Fig. 4(a), which was first developed by Clyde Stauffer in 1964 as a means for measuring interfacial tension between two fluids (Stauffer 1965). By measuring the droplet radii and the tangent slopes on the droplet perimeter, a non-dimensional shape factor β can be ascertained (Eq. 11). The surface tension is a product of the volume of the droplet, the difference in fluid densities, and the forces of gravity applied to the droplet (Eq. 12).

$$\frac{1}{R}+\frac{\sin\phi}{X}=2+\beta\cdot Y \tag{11}$$

$$\gamma=\frac{g\cdot(\rho_1-\rho_2)\cdot N^2}{\beta} \tag{12}$$

R droplet radius from the drop center to the bottom

X and Y coordinates of the tangent line where the slope Φ is measured

Table 1 Data from pendant drop experiments of Halocarbon oil in water/alcohol

Sample	Droplet radius (mm)	B	Δρ (g/mL)	*X*, *Y*, Φ (mm, mm, °)	IF (mJ/m^2)
Oil–Water	1.78	−0.0187	0.95	60.4, 110, 73.4°	50.5
Oil+(50% Ethanol)	0.91	−0.0807	1.05	26.2, 58.4, 74.4°	17.3
Oil+(50% Methanol)	1.14	−0.0605	1.04	45.6, 56.2, 82.4°	21.4

Table 2 Simulated interfacial tensions for pad geometries in water, and dilute alcohol

Pad	Simulation	Surface energy (J)	Surface area (m^2)
Rectangle pad	Embryo, Oil, Water	-2.72×10^{-9}	2.52×10^{-7}
Rectangle pad	Embryo, Oil, 50% EtOH	-7.44×10^{-10}	2.47×10^{-7}
Rectangle pad	Embryo, Oil, 50% MethOH	-9.37×10^{-10}	2.48×10^{-7}
Truncated cross	Embryo, Oil, Water	-2.03×10^{-9}	2.32×10^{-7}
Truncated cross	Embryo, Oil, 50% EtOH	-5.44×10^{-10}	2.27×10^{-7}
Truncated cross	Embryo, Oil, 50% MethOH	-6.84×10^{-10}	2.28×10^{-7}
Elliptical pad	Embryo, Oil, Water	-5.25×10^{-9}	2.30×10^{-7}
Elliptical pad	Embryo, Oil, 50% EtOH	-1.61×10^{-9}	2.25×10^{-7}
Elliptical pad	Embryo, Oil, 50% MethOH	-2.00×10^{-9}	2.26×10^{-7}

ρ_1 and ρ_2 fluid density of the droplet and external fluid
g gravitational constant
N length of the needle inner diameter

The pendant drop experiment was recorded using a goniometer setup (First Ten Angstroms, Model #FTA200). A 5 mL plastic syringe filled with Halocarbon oil was mounted on the goniometer, and a 19-gauge-needle without bevel was dipped into the experimental solution. Incremental pressure was applied to the syringe plunger until a well formed pendant drop was visible (Fig. 4(b)). The pendant

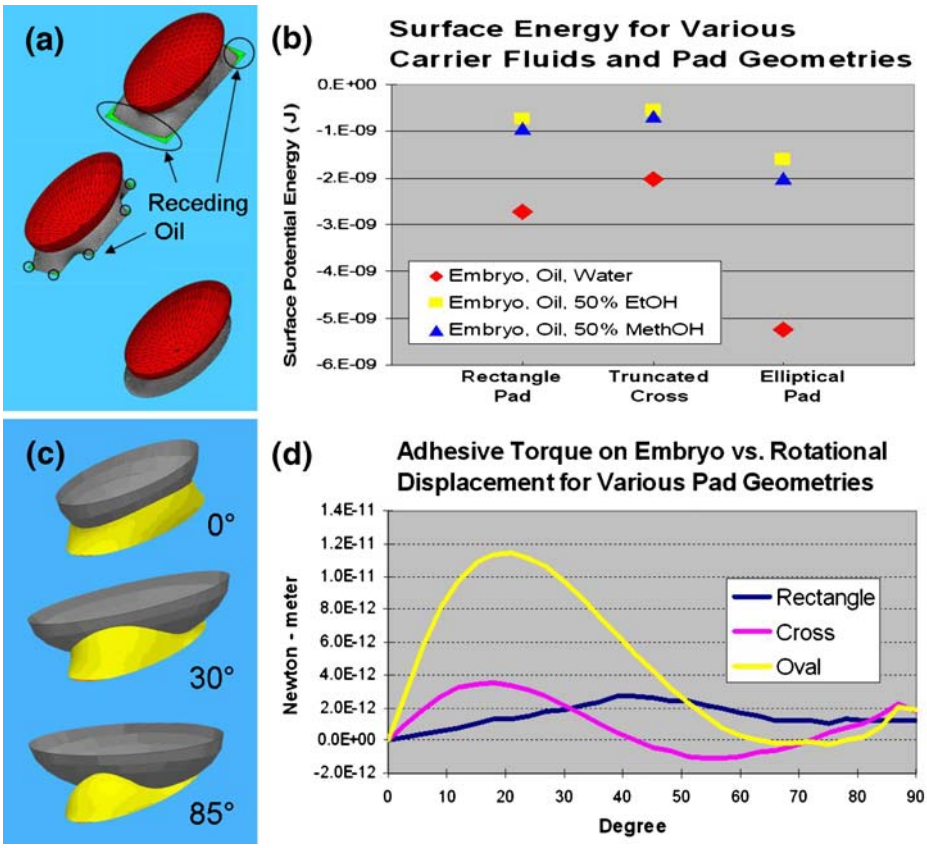

Fig. 5 Surface Evolver simulations of an embryo on an adhesive pad. (**a**) Linear translation of embryo on various geometries. Surface Evolver models of embryos on the three pad geometries in 50% ethanol solution. Oil is receding from the edges of the pads because of a smaller interfacial energy between the oil and the ethanol. Simulations performed include the *rectangular pad*, *truncated cross pad*, and *elliptical pad*. The *elliptical pad* had the most surface area covered submerged in alcohol. (**b**) Simulated surface energy of three pad geometries demonstrating the highest stability of the embryo on the *elliptical pad*, and the lowest stability on the *truncated cross pad* for all three carrier fluids. (**c**) Surface Evolver depictions of oil surface in relation to rotated embryo for the *elliptical pad*. (**d**) Simulated Torque from adhesive oil on embryo when embryo is rotated from the orientation of maximum overlap (0°) up to 90° rotation for the three pad geometries. The *oval pad* has the largest effect on the embryo and the *rectangle* has the least effect regarding maximum torque amplitude

drop experiments performed are: oil in water, oil in 50 and 95% ethanol, and oil in 50 and 95% methanol. The purer alcohols (95% ethanol, 95% methanol) were not compatible with the pendant drop method because the interfacial tension was too small to form a droplet. The pendant drop calculations (Table 1) confirm that the oil in water has the highest interfacial tension of 50.5 mJ/m^2, oil in 50% methanol has the second highest interfacial tension of 21.4 mJ/m^2, and oil in 50% ethanol has the lowest interfacial tension of 17.3 mJ/m^2.

Using the interfacial energy conditions, we compared three different pad geometries under three different fluidic conditions (Table 2). The Surface Evolver simulation takes into account the oil interface with the SAMs pad, the carrier fluid, and the embryo membrane. The SAMs-Oil-Water contact angle and Embryo-Oil-Water contact angles were measured to be 25 and 31° respectively. The SAMs-Oil-Alcohol contact angle and Embryo-Oil-Alcohol contact angles were estimated to be 30 and 39° respectively.

The results from the Surface Evolver simulations show that the embryos are most stable (surface potential energy= -5.25×10^{-9} J) on the elliptical pad with water as a carrier fluid and most unstable on the truncated cross pad with 50% ethanol (surface potential energy=-5.44×10^{-10} J). In general, the embryos have relatively lower surface potential energy in water than in the alcohol on all three pad geometries. The elliptical pad has lowest surface potential energy in all three carrier fluids, while the cross pad has the highest. It can be explained by the observation made from the surface area; the surface area of the oil retreats the most on the truncated cross than it does on the other two pads, and this can be visualized by the physical exposure of pad to alcohol (Fig. 5(a),(b)). The more exposed pad area to the carrier fluid results in higher surface energy and less stability of the embryo assembly.

Torque on a rotated embryo was also simulated for the rectangle, oval, and truncated-cross pad geometries. This simulation demonstrated the ability for the embryo to be automatically oriented based on the oil adhesive torque of the assembly pad (Fig. 5(c),(d)). The results of this simulation illustrate three distinct trends: (1) The rectangular pad has the smallest restoring torque with a 2.70×10^{-12} Nm peak at 39° rotation; (2) The truncated-cross pad has a sinusoidal pattern with a positive peak (3.55×10^{-12} N-m) at 18° rotation and a negative peak (-1.06×10^{-12} N-m) at 57° rotation; and (3) the oval pad has the strongest restoring torque (1.14×10^{-11} N-m) at 20° rotation.

4.1.2 Embryo deposition

The experimental setup is shown in Fig. 6(a) and (b). During embryo assembly, the microchannel is placed under a stereoscopic dissecting microscope (Leica, Wild M10). The source of flow during assembly is a 5 mL glass air-tight syringe (Hamilton Co., #81530) attached to a micrometer clamped together in a homemade aluminum stand. The port of the microfluidic device is cored using a 17-gauge-needle which is compatible with 24-gauge-Teflon-tubing (Weicowire, #TS-24). The Teflon tubing is also securely fastened to a 22-gauge-needle of the micrometer syringe. A single revolution of the micrometer syringe provides 500 microns of displacement to the syringe plunger, which results in approximately 50 picoliters of fluid.

Two primary microscopes are used to perform the characterization and biological observation within the microchannels. A confocal laser scanning microscope (Leica, TCS-SP2) magnifies the thermal flows in the microchannel using fluorescence thermometry. A microscope with differential interference contrast (DIC) optics (Zeiss, Axiovert 200) is used to observe the morphogenetic movements of the embryo during development. Both microscopes are connected to separate personal computers (PC) with commercial image capture software developed by their respective companies for scanning and time-lapse recording.

Thermal flows are prepared by heating/cooling baths of solution using a two position electronic chilling/heating dry bath (Torrey Pines Scientific, Model IC22). An external thermometer with probe is used to verify average bath temperature. To drive the flows, we use a four channel peristaltic pump with Polyvinyl Chloride tubing (Rainin Corporation, Model Dynamax RP-1). The inlets and outlets of the peristaltic pump tubing are fitted around Teflon tubing to draw fluids from the bath, into the microfluidics device. All input and output Teflon tubing for the various channels are the same length from source to destination. We attempted to make this distance as short as possible to reduce heat loss; however, this distance is longer than desired because of the microscope and peristaltic setup. Flow setups are identical between the two microscopes.

4.1.3 Embryo self-assembly

The ability to attach and detach embryos inside the microchannel is the primary contribution of this research. Attachment can be measured by observing the ratio of the embryos that assemble inside the microchannel versus the total amount of embryos attempted. It can also be measured by the total time it takes to assemble one embryo within the microfluidic channel. Both methods were performed and the results recorded.

The microfluidic assembly and subsequent time-lapse imaging of *Drosophila* embryos requires the embryos to have their chorions removed. Embryos are dechorionated in a 50% bleach solution and rinsed in an embryo wash buffer

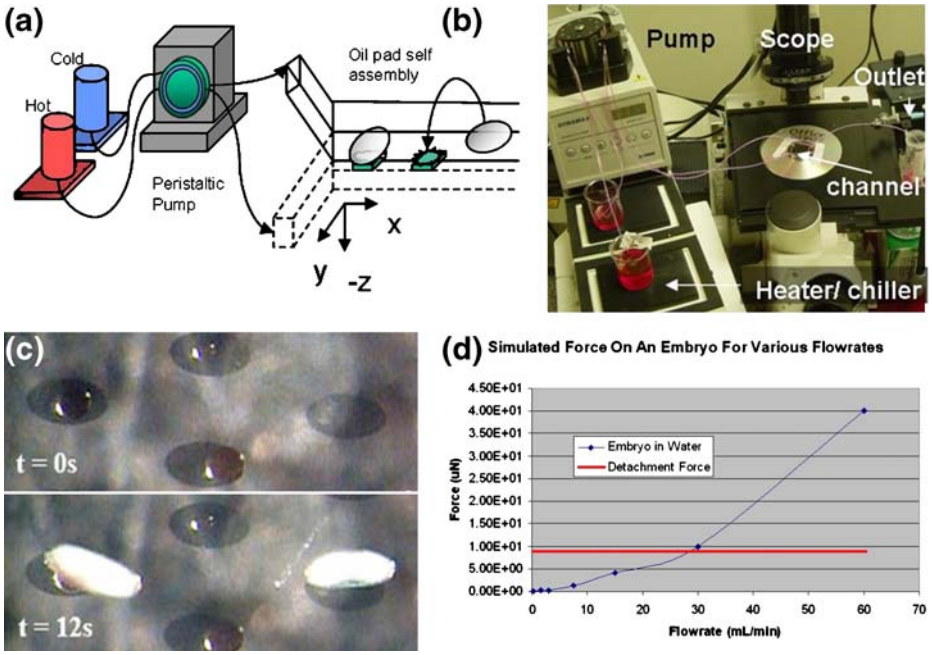

Fig. 6 Embryo assembly experimental setup and calibration. (**a**) Diagram of peristaltic pump setup for thermal perturbation. (**b**) Photograph of thermal profile calibration using fluorescence thermometry with Rhodamine B with confocal microscope. (**c**) Self-assembly of two embryos on oval pads over a 12 s time period. Flow is going from left to right at 50 μm/s. (**d**) Calibration of force on embryo (simulated) for various flow rates vs. the detachment force of an embryo on a 400×200 μm pad in water

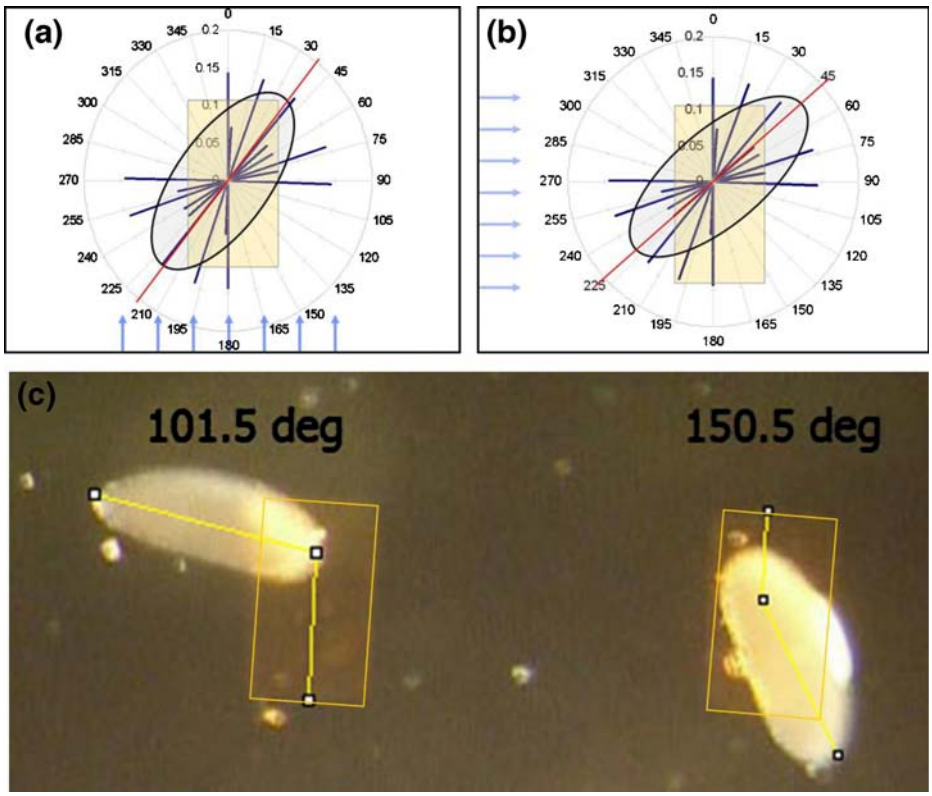

Fig. 7 Embryo orientation on pads after assembly. (**a**) Radar graph of normalized embryo assembly orientation data for pads oriented inline with flow. (**b**) Radar graph of normalized embryo assembly orientation data for pads oriented perpendicular to flow. Average orientation is indicated with the line bisecting the radar graph at 36±1° and 46±1° respectively. (**c**) Examples of orientation measurements of embryos on self-assembly pads using ImageJ software

(0.7% NaCl/0.003% Triton X-100) prior to assembly and imaging. A syringe is pre-filled with an alcohol dilution prior to picking up embryos from the wash buffer. This alcohol carrier fluid (50% ethanol or 50% methanol) acts as a surfactant during the assembly process by reducing the interfacial tension. The effects of ethanol and methanol on embryo viability was also studied, and it was demonstrated that methanol is a favorable carrier fluid that has little effect on embryo growth under our conditions. Embryos are introduced manually into the microchannel by rotating the micrometer very slowly. The embryos enter the chamber flow in a straight path unless they bump into other embryos that are floating in the channel or that have already attached to a pad. The estimated flow velocity during attachment ranges around 50 μm/s (Fig. 6(c)). Once a sufficient number of embryos are attached, the channel is flushed with a buffer solution. Because water has a higher interfacial tension with the oil bridge, the embryos adhere to the oil adhesive more firmly.

4.1.4 Detachment of embryos

The detachment of embryos is dependent on the embryo pad geometry, fluid shear, and the interfacial tension between the buffer solution and the oil bridge. From previous research, it was shown that 400×200 μm rectangular pads require approximately 8.9 μN of shear force to detach the embryo using fluid flow in an aqueous carrier fluid (Bernstein et al. 2002). By simulating fluid force on an embryo using Fluent®; it is found that it would take a flow rate of approximately 25 mL/min to detach the same embryo inside a microfluidic channel (Fig. 6(d)).

At the maximum flow rate of our peristaltic pump, the embryos held firmly to the pad at a velocity of 8 mL/min. Typical operating flow rates are between 0–4 mL/min, therefore, it is beneficial to either shrink the pad geometries or reduce the environmental interfacial tension by using an alcohol buffer. Using an alcohol buffer, it only takes 50–100 μL/min to dislodge the embryo from the pad. This corresponds to a detachment force of only 2–4 pN of pressure, a force reduction of over three orders of magnitude.

4.1.5 Embryo orientation after assembly

The orientation of embryos assembled onto the oil-adhesive pads is directly related to the pad geometry. For this experiment, we measured the absolute value of angle displacement from the greater ellipsoidal axis of the embryo compared to the base line of the assembly pad base. Approximately 75 embryos were measured, and their results compiled in the following graphs (Fig. 7(a),(b)). For this experiment, 200×400 μm rectangular and elliptical pad geometries were used because the truncated cross geometry demonstrated poor overall performance in assembly. Embryos assembled onto pads inline with flow averaged a smaller orientation offset (36°) than those assembled onto pads perpendicularly oriented to flow (46°). In the radar graph below, the data quadrants II and IV are combined into quadrants I and III to depict the absolute offset of embryo-pad orientation. The measuring tool for this experiment was ImageJ complimentary of the National Institute of Health (Abramoff et al. 2004; Girish and Vijayalakshmi 2004). Images of embryos assembled onto pads were taken from

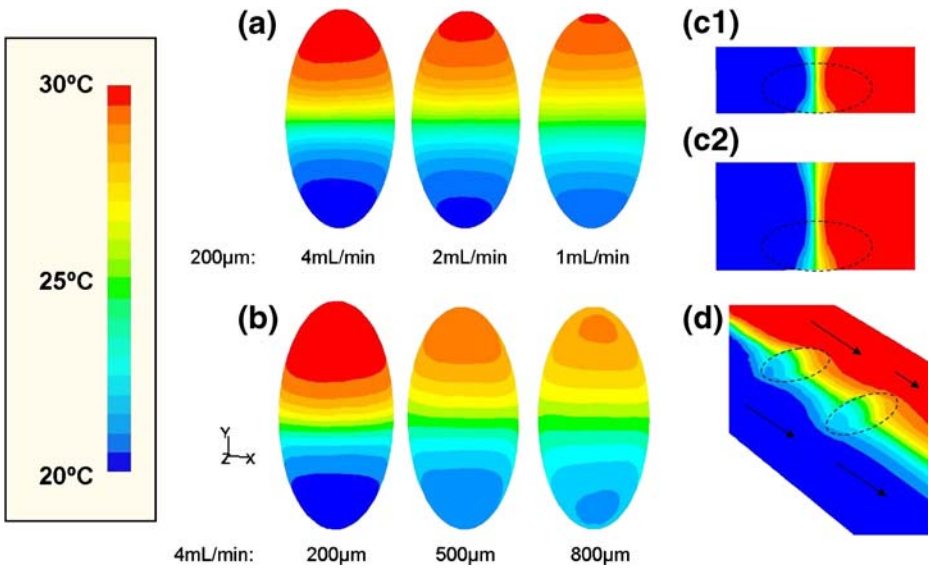

Fig. 8 Simulated binary thermal profile across single embryo. Simulations of binary thermal profile in Y-junction microchannels. (**a**) Thermal profile for various velocities: 4, 2, and 1 mL/min with embryo at 200 μm from the junction. (**b**) Thermal profile vs. *x*-displacement from junction; embryos at 200, 500, and 800 μm with binary flows at 4 mL/min. (**c**) Thermal profile vs. channel height; embryos have a narrower gradient in shorter channels. (**d**) Multiple embryos in a channel at displacements of 200, and 500 μm

collected self-assembly recordings. An example of an embryo orientation measurement is shown (Fig. 7(c)). Successful orientation was determined if the anterior/posterior axis of the embryo was inline with the adhesive pad.

4.2 Thermal perturbation

Thermal perturbation was analyzed in three different ways: simulation, labeled thermal flow characterization, and embryo development experimentation. The simulation of temperature inside the microfluidic channels was performed using Fluent® to determine the best channel geometry to narrow the temperature gradient around the embryo. The experimental characterization of temperature was performed using Rhodamine B dye via fluorescence thermometry. Because heating and cooling of the fluids occur externally to the device, the bath temperatures and flow rates were calibrated to obtain specific profiles inside the device. Observation of wild type embryos immobilized in a microfluidic device by time-lapse DIC microscopy demonstrates the effect of thermal perturbation on development and embryo morphology.

4.2.1 Simulation of temperature gradients

Temperature profile simulations were performed using Fluent® Computational Fluid Dynamics (CFD) software. One set of simulations includes the embryo with the dorsal/ventral side facing the fluid flow, and the other set of simulations directed flow at the anterior/posterior side of the embryo. The simulations were modeled in three dimensions, using the material properties of water to estimate thermal diffusion through the embryo. Variables of simulation included channel dimensions, flow rate, and embryo placement.

Observations from the simulations reveal many characteristics useful for optimizing microfluidic thermal perturbation. Firstly, the thermal profile narrows by 50% as the binary flow rate doubles (Fig. 8(a)). Also, thermal profiles around an embryo widen by 85% as the displacement from the junction increases from 200 to 800 μm (Fig. 8(b)). Because the microchannel undergoes heat loss from the top and bottom, the narrowest diffusion zone is in the middle of the channel (Fig. 8(c)). Therefore, shorter channels expose the embryo to the narrowest profile. In terms of high throughput, multiple embryos placed in the channel at

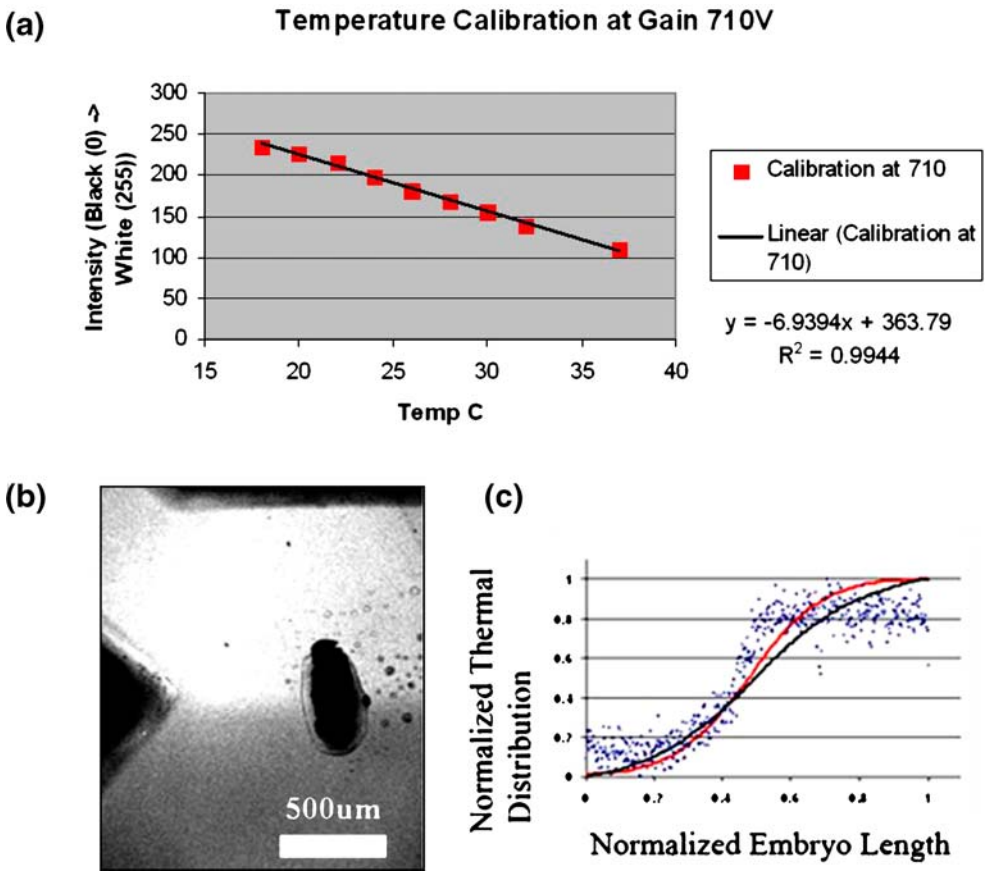

Fig. 9 Measured thermal profile across self-assmbled embryo in microfluidic channel. (**a**) Temperature calibration of Rhodamine B dye vs. 8-bit monochromic intensity. Relationship is very linear demonstrating that as the dye warms, the fluorescence decreases. (**b**) Fluorescent dye in a microchannel around an embryo assembled to an oil pad. Micrograph of optical wavelengths of dye around embryo. Temperatures depicted are 20°C (*light*) and 30°C (*dark*). Specks of oil are seen to the right of the immobilized embryo. (**c**) Normalized thermal distribution over the length of the embryo for experimental (*filled circle*) and simulation results at 4 mL/min (*gray line*) and 1 mL/min (*black line*) for (27→20°C). These results are in good agreement

Table 3 Cycle duration of embryos within microchannels at 24°C against 4 mL/min flow rates

Nuclear cycle	10	11	12	13	14
Open substrate cycle duration (min) (Foe and Alberts 1983)	11.1	12.5	15.7	26.2	65
Microchannel cycle duration (min) (this study)	10.5	11.8	14.3	22.6	62.3

displacements of 200, 500, and 800 μm from the Y-junction have profiles that are only 2% wider than that of embryos at the same displacements in isolation (Fig. 8(d)).

4.2.2 Experimental characterization of temperature

The binary flow temperatures inside the device are verified experimentally with fluorescence thermometry using Rhodamine B dye. Rhodamine B is capable of being a thermo-indicator because its photoluminescence quantum efficiency (Φ) is dependent on temperature. As long as the dye concentration is kept constant, fluorescence activity will be completely dependent on temperature (Eq. 13).

$$I = ALC\varepsilon\phi \tag{13}$$

I emission intensity
A detection efficiency
L incident laser intensity
C dye concentration
ε absorption coefficient

Calibration of the Rhodamine B dye is a two step process. The first step involves the measuring of dye fluorescence at a given set of temperatures. For this step we use a microscope slide incubator (Harvard Apparatus, PDMI-2), and a microscope fluorescence scanner to set to a particular gain of 710 V (Fig. 9(a)). Two problems were identified when using Rhodamine B dye. The first problem is that Rhodamine B dye absorbs readily into PDMS. This problem was addressed by allowing the walls of a microfluidic device to saturate with the Rhodamine B dye after a period of 30–60 min. The second problem was that for each temperature, the gain changed the intensity reported in an unparallel fashion. Therefore, each gain voltage requires a new calibration curve of temperature vs. gain to accurately measure the temperature in-channel.

Once the intensities are calibrated for a particular gain, the temperatures inside the channel must be calibrated for given flow rates using particular bath temperatures. The temperatures inside the channel for a given flow rate also depend on the length of the capillaries connecting the baths to the device. Also, the room temperature will also slightly affect the heat loss from the capillaries to the device. For our experiments, we chose two temperatures, 20 and 30°C, to calibrate at 4 mL/min flow rate and compared the normalized data results from the thermal profile tangential to the flow in front of the embryo with the simulated results (Fig. 9(b),(c)). These thermal profile results are in good agreement.

4.2.3 Thermal perturbation of embryos

Two sets of experiments determined the effects of thermal perturbation on *Drosophila* embryos. First, we allowed wild type embryos to develop in a microfluidic device with flow shear of 4 mL/min at 24°C and observed development using time-lapse microscopy. Second, we subjected embryos to thermal perturbation by allowing embryos to develop in a microfluidic device with binary flow of two different temperatures.

Early *Drosophila* embryos develop as a syncytium with 13 rapid, synchronous nuclear divisions in the absence of cytokinesis. Nuclei migrate to the cortex of the embryo by

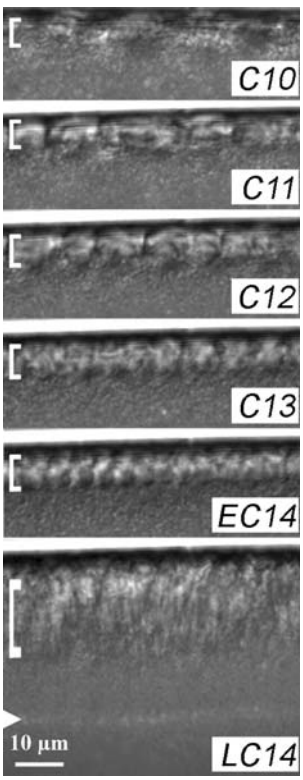

Fig. 10 Early *Drosophila* embryos undergo normal development within microfluidics channels under standard conditions. Sequential frames of a representative time-lapse DIC movie of an embryo developing with 4 mL/min flow. Nuclear cycle is indicated in the corner of each image. The last two images represent early (EC14) and late (LC14) cellularization. *Arrow head* indicates the position of the furrow front. *Bracket* specifies the location of nuclei

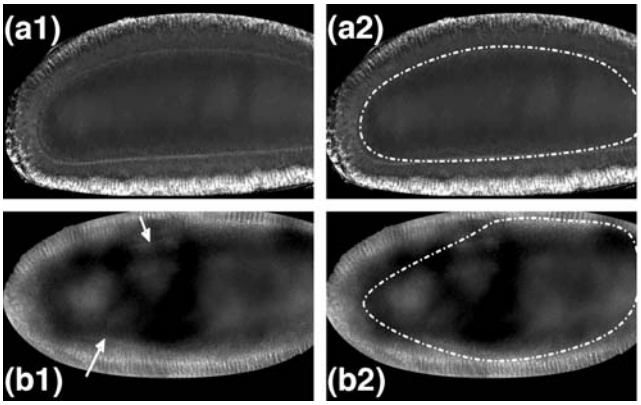

Fig. 11 Binary temperature gradient disrupts cellularization. Images show embryos during the onset of cellularization. The *left column* (a1), (b1) are the raw images with the background cut out. The *right column* (a2), (b2) are the same images with the furrow front highlighted with a *dashed line*. (**a**) Control experiment displaying the furrow front (contractile apparatus) in the channel. The membrane furrow front is concentrically even across the embryo as the embryo is developed in an environment of 24°C. (**b**) The thermally perturbed embryo with the posterior-hot (30°C) and the anterior-cold (20°C). The membrane furrow front is more advanced on the warm posterior than the cold anterior, indicative of abnormal asynchronous growth

nuclear cycle 10, where they undergo four additional syncytial divisions. During interphase of the 14th nuclear cycle, plasma membrane furrows encapsulate the cortically positioned nuclei through a special form of cytokinesis called cellularization. The timing of these nuclear cycles and the process of cellularization are highly reproducible events and can be visualized using DIC microscopy. For these reasons, we chose to study these events in embryos developing in microfluidic devices and subjected to thermal perturbation.

First, we observed the effect of the fluid shear (4 mL/min) on embryo development at 24°C. The channel dimensions are 1,000 μm wide by 500 μm deep providing a relative velocity of 1.33 cm/s. The relative fluid shear is approximated as 0.2 $\mu N/m^2$, and it was not expected that the fluid shear would be an issue. Quantification of nuclear cycle times, shown in Table 3, indicates that embryos subjected to fluid flow in microfluidic channels during syncytial nuclear divisions and cellularization develop at rates similar to embryos developing on the surface of glass coverslips in oil (Foe and Alberts 1983). In addition, we did not detect any morphological defects in the embryos subjected to fluid flow as indicated by normal cortical nuclear morphology during the syncytial divisions and normal rates of furrow ingression during cellularization (Fig. 10).

To observe any effects of thermal perturbation on embryo development, embryos were immobilized in the microchannel, and binary thermal flows were introduced into the channel with temperatures of 20 and 30°C, where the anterior of the embryo was at 20°C and the posterior was at 30°C. The embryos were visualized by time-lapse microscopy, and the general morphology of the embryos was assessed from nuclear cycle 10 through cellularization. The synchronous advancement of the membrane furrows during cellularization was abnormal. The furrow front in the posterior end of the embryo, developing at 30°C, advanced at a faster rate than the furrow front at the anterior end, developing at 20°C (Fig. 11). This observation shows that thermal perturbation by binary flow of two different temperatures over a developing *Drosophila* embryo can affect cellularization.

5 Conclusions and summary

In this paper, a microfluidic device was created capable of efficiently delivering binary thermal flows across well positioned embryos. In-channel oil adhesive pads were fabricated using patterned gold pads covered in self-assembled monolayers (SAMs). *Drosophila* embryos were introduced into the microfluidic channel, and attached to the oil pads with an alcohol based surfactant. Removing the alcohol surfactant from the device increased the embryo adhesion to the oil pad by three orders of magnitude (detachment with surfactant: 0.1 mL/min; detachment without surfactant: ~25 mL/min). Therefore, the embryos could be locked in place by removing the alcohol surfactant for high flow rates necessary for sharp thermal gradients. The adhesion of the embryo and oil bridge to the SAMs covered substrate was simulated and experimentally characterized in both aqueous and alcohol flow environments. Reintroducing alcohol into the microchannel decreased the interfacial tension and the embryo detached from the pad with as little as 50–100 μL/min flow rates. We demonstrated that a thermal gradient applied across live *Drosophila* embryos dramatically disrupts primary epithelial cell formation. This process depends on microRNA-mediated translational control, cytoplasmic ribonucleoprotein body function, polarized membrane secretion and cytoskeletal dynamics.

Genome-wide screening relies on accurate and extensive data collection to characterize signaling pathways in biochemical networks. Improvements in tool accuracy and automation will further shed light on complex signaling interactions induced by signal inhibition, gene mutation, and environmental perturbation. This device has a great potential beyond thermal perturbation, such as screening large chemical libraries on cells for desired effects on cell morphology. These experiments all benefit from high throughput low-volume microfluidic handling tools to expedite existing assays for analyzing molecules, cells and embryos.

Acknowledgements We would like to thank Welch Foundation, SPRING, and the Center for Nano and Molecular Science and Technology (CNM) at UT Austin for their facilities including the goniometer setup. We would also like to thank Professor Grant Wilson and Dr. Peter Carmichael for their discussions on surfactants and interfacial tension, and Ashwini Gopal for facilitating the fabrication of the self-assembly pads suitable for DIC imaging. This study was supported in part by the March of Dimes Basil O[1]Connor Award and the National Institute of Health, grant RO1GM067013 (to J.C.S) and the National Science Foundation Nanoscale Exploratory Research Program ECS-0609413 (to X.J.Z).

References

M.D. Abramoff, P.J. Magelhaes et al., Biophoton. Int. **11**(7), 36–42 (2004)
J.R. Anderson, D.T. Chiu et al., Anal. Chem. **72**(14), 3158–3164 (2000)
R.W. Bernstein, X.J. Zhang et al., *μTAS* (Nara, Japan, 2002)
K. Brakke, *Surface Evolver is an Interactive Program for the Modeling of Liquid Surfaces Shaped by Various Forces and Constraints* (Mathematics Department, Susquehanna University, Selinsgrove, PA, 2005)
T.D. Brown, J. Biomech. **33**(1), 3–14 (2000)
R.W. Carthew, Curr. Opin. Cell Biol. **13**(2), 244–248 (2001)
F. Caruso, H. Lichtenfeld et al., J. Am. Chem. Soc. **120**(33), 8523–8524 (1998)
D. Debarre, W. Supatto et al., Opt. Lett. **29**(24), 2881–2883 (2004)
A. Eldar, B.Z. Shilo et al., Curr. Opin. Genet. Dev. **14**, 435–443 (2004)
J. Fang, K.F. Böhringer, J. Micromechanics Microengineering **16**, 721–730 (2006)
V. Foe, B.M. Alberts, J. Cell Sci. **16**(1), 31–70 (1983)
E. Freire, T. Coelho-Sampaio, J. Biol. Chem. **275**(2), 817–822 (2000)
V. Girish, A. Vijayalakshmi, Indian J. Cancer **41**(1), 47 (2004)
B.A. Grzybowski, X. Jiang et al., Phys. Rev. E Stat. Nonlin. Soft. Matter. Phys. **64**(1 Pt 1), 011603 (2001)
Halocarbon-Products-Corporation Frequently Asked Questions, about Halocarbon 700 (2006)
A. Hatch, A.E. Kamholz et al., Nat. Biotech. **19**(5), 461–465 (2001)
R.F. Ismagilov, A.D. Stroock et al., Appl. Phys. Lett. **76**(17), 2376–2378 (2000)
A.E. Kamholz, B.H. Weigl et al., Anal. Chem. **71**(23), 5340–5347 (1999)
K. Kendall, J. Phys. D: Phys. **4**, 1186–1195 (1971)
E.M. Lucchetta, J.H. Lee et al., Nature **434**(7037), 1134–1138 (2005)
E.M. Lucchetta, M.S. Munson et al., Lab. Chip. **6**(2), 185–190 (2006)
Microchem-Corporation. SU8-2000 Photoresist Technical Literature. (2006)
J. Niemuth, R. Wolf, Dev. Genes Evol. **204**(7–8), 444–452 (1995)
C. Nusslein-Volhard, E. Wieschaus, Nature **287**(5785), 795–801 (1980)
S.R. Oliver, T.D. Clark et al., J. Am. Chem. Soc. **123**(33), 8119–8120 (2001)
N.A. Peppas, J.J. Sahlin, Biomaterials **17**(16), 1553–1561 (1996)
G.M. Rubin, E.B. Lewis, Science **287**(5461), 2216–2218 (2000)
U. Srinivasan, D. Liepmann et al., J. MEMS **10**(1), 17–24 (2001)
C.E. Stauffer, J. Phys. Chem. **69**(6), 1933–1938 (1965)
M. Sugihara-Seki, Biorheology **37**(5–6), 341–359 (2000)
M. Sugihara-Seki, Biorheology **38**(1), 3–13 (2001)
J.J. Talghader, J.K. Tu et al., IEEE Photonics Technol. Lett. **7**(11), 1321–1324 (1995)
G.M. Walker, H.C. Zeringue et al., Lab. Chip. **4**(2), 91–97 (2004)
X. Xiong, Y. Hanein et al., J. MEMS **12**(2), 117–127 (2003)
H.J. Yeh, J.S. Smith, IEEE Photonics Technol. Lett. **6**, 706–708 (1994)
G. Yucel, S. Small, Curr. Biol. **16**(1), R29–R31 (2006)
X.J. Zhang, C.-C. Chen et al., J. MEMS **14**, 1187–1197 (2005)